

W. Song, C. Xu*, M.P. Smith, A.R. Chakhmouradian, M. Brenna, J. Kynický, W. Chen, Y. Yang, M. Deng, and H. Tang, 2018, Genesis of the world's largest rare earth element deposit, Bayan Obo, China: protracted mineralization evolution over ~1 billion years: Geology, <https://doi.org/10.1130/G39801.1>.

1 **Analytical Methods**

2 **Whole-rock analysis**

3 Major and rare earth element abundances in drill core samples were
4 determined by a Spectro Blue Sop inductively coupled plasma optical emission
5 spectrometer (ICP-OES) at the School of Earth and Space Sciences, Peking
6 University. The analytical precision is $\pm 5\%$ for all the elements.

7

8 **Element mapping**

9 Compositional X-ray maps of monazites were obtained with an Oxford
10 INCA X-MAX50 250+, energy dispersive X-ray spectrometer installed on a FEI
11 Quanta-650FEG scanning electron microscope, at the School of Earth and
12 Space Sciences, Peking University. The backscattered electron and
13 energy-dispersive X-ray data acquired from the samples were combined and
14 processed automatically to generate the most sensitive X-ray mapping. The
15 sample, coated with a conductive Cr layer (10 nm thickness) to prevent sample
16 charging, was analyzed in a high-vacuum mode at standard operating
17 conditions (accelerating voltage of 20 kV, probe current 5 nA).

18

1 **Monazite dating**

2 Monazite grains ranging from 50 to 100 μm across were collected from the
3 drill core using conventional heavy liquid separation techniques.
4 Back-scattered electron images show that the crystals are compositionally
5 homogeneous and free of inclusions. The Th-Pb dating of monazite was
6 performed using a Cameca IMS-1280 secondary-ion mass-spectrometer
7 (SIMS) at the Institute of Geology and Geophysics (IGG), Chinese Academy of
8 Sciences (CAS). During the analysis, an O^{2-} primary ion beam was
9 accelerated at 13 kV with an intensity of ca. 2-3 nA. Aperture illumination mode
10 (Kohler illumination) was used with a 200- μm primary beam mass filter
11 aperture to produce even sputtering over the entire analyzed area. The
12 ellipsoidal spot was about $20 \times 30 \mu\text{m}$ in size. Positive secondary ions were
13 extracted with a 10 kV potential. Monazite 44069 was used as a standard. A
14 ^{207}Pb -based common Pb correction method was used. Further instrumental
15 and analytical details can be found in Li et al. (2013).

16

17 **Trace element analysis**

18 In-situ laser-ablation analyses of dolomite and apatite in thin sections were
19 performed by inductively-coupled-plasma mass-spectrometry (ICP-MS) at the
20 School of Earth and Space Sciences, Peking University, using a COMPexPro
21 102 excimer laser and an Agilent7500ce/cs mass-spectrometer. The diameter
22 of an ablation spot was 32 μm . The NIST 610 glass was used as a calibration

1 standard, and the Ca content measured by electron-microprobe analysis, as
2 an internal standard. Signal intensity for indicative trace elements was
3 monitored online during the analysis to ensure that the ablation spot was
4 confined to the area of interest and did not sample other mineral phases or
5 inclusions. The analytical error was estimated to be better than 5% at the ppm
6 level.

7

8 **Nd-Sr isotopic analysis**

9 The Nd isotopic composition of monazite was measured in situ by
10 multi-collector ICP-MS using a Thermo-Finnigan Neptune instrument coupled
11 to a 193-nm ArF excimer laser-ablation system at the IGG, CAS. The diameter
12 of a laser spot and frequency were adjusted to between 10-24 µm and 4-10 Hz,
13 respectively, depending on the Nd concentration in the sample. Each spot
14 analysis consisted of approximately 60 s of signal acquisition. More detailed
15 information on the in-situ Nd isotopic analysis employed in the present work is
16 available in Yang et al. (2008). The Sr isotopic compositions of dolomite and
17 apatite were measured in situ by laser-ablation multicollector ICP-MS
18 (Resonics + Nu instruments) at the State Key Laboratory of Geological
19 Processes and Mineral Resources, China University of Geosciences (Wuhan).
20 The isotopic ratios were quantified in a static multicollector mode at low
21 resolution, using seven Faraday collectors and a mass configuration array
22 from ^{82}Kr to ^{88}Sr to monitor variations in Kr, Rb and Sr signals. The detailed

1 analytical procedure and data-reduction strategy are described in Tong et al.
2 (2015).

3

4 **Figure captions for Data Repository**

5 Figure DR1. Geological sketch map of the Bayan Obo deposit. a: The
6 locations of Bayan Obo and ~1.3 Ga mafic dikes in the northern North China
7 Craton (NCC; Yang et al., 2011; Zhang et al., 2012; Wang et al., 2014); b: The
8 locations of drill core, carbonatite and mafic dikes in Bayan Obo.

9 Figure DR2. Drill core samples and their photomicrographs. a, b: Drill cores
10 collected from the Eastern Orebody at a depth of 1776 m. c: Photomicrograph
11 of dolomite (Dol) showing re-crystallization texture with the development of
12 elongation and preferred orientation, and triple junctions between crystals.
13 Rare earth minerals (REM) of monazite and REE-fluorocarbonates occur as
14 veinlets. d: Photomicrograph of primary fine-grained dolomite as a matrix to
15 porphyritic dolomite. Disseminated REM is associated with fluorite (Fl).

16 Figure DR3. Plot showing the total light REE_2O_3 contents (La-Sm) of the drill
17 core samples with vertical depth.

18 Figure DR4. X-ray compositional maps of representative monazite grains.

19 Figure DR5. Compositional variation of primary and recrystallized dolomite
20 (Dol) and apatite (Ap) from the Bayan Obo drill cores. a: La/Yb_{cn} (cn -
21 chondrite normalized) vs. total REE; b: Y/Ho vs. Eu/Eu^* (Eu anomaly).

22 Figure DR6. Revised tectonic discrimination diagrams for mafic dikes from the

1 northern NCC. Data of the Wulahada and Wudalianchi volcanic fields in NCC
2 are plotted as reference for cases of basaltic magmatism with the source
3 influenced by previous subduction events (Wulahada at 142 Ma; Zhang et al.,
4 2003) and for purely intraplate (OIB-like) volcanism from an enriched source
5 (Wudalianchi at 10 Ma to recent; Zhang et al., 1995). The
6 Mid-Mesoproterozoic mafic dikes (Zhang et al., 2012; Wang et al., 2014) in
7 northern NCC plot in both IAB and OIB, and Bayan Obo data (Wang et al.,
8 2003; Yang et al., 2011) mostly in the IAB field, indicating influence of
9 subduction derived fluids in their mantle source. The tectonic discrimination
10 diagrams are from Vermeesch (2006). OIB, Ocean Island Basalt; IAB, Island
11 Arc Basalt; MORB, Middle Ocean Ridge Basalt.

12 Figure DR7. Primitive mantle normalized diagram for mafic dikes from the
13 northern NCC. Data of OIB is from Sun and McDonough (1989), IAB based on
14 average compositions reported by Jakes and Gill (1970), McCulloch and
15 Gamble, (1991), and with dashed Ta abundance based on the Nb/Ta ratios
16 reported by Stolz et al. (1996). Additional data sources are same as Fig. DR6.
17 Note that the Bayan Obo mafic rocks have Nb, Ta and Ti negative anomalies
18 and Pb and Sr positive anomalies resembling IAB, and have mostly lower
19 elemental abundances than OIB, suggesting a subduction influence in their
20 genesis.

21

22 **References for Data Repository**

- 1 Jakes, P., and Gill, J., 1970, Rare earth elements and the island arc tholeiitic
2 series: Earth and Planetary Science Letters, v. 9, p. 17-28.
- 3 Li, Q.L., Li, X.H., Lan, Z.W., Guo, C.L., Yang, Y.N., Liu, Y., and Tang, G.Q.,
4 2013, Monazite and xenotime U-Th-Pb geochronology by ion microprobe:
5 dating highly fractionated granites at Xihuashan tungsten mine, SE
6 China: Contributions to Mineralogy and Petrology, v. 166, p. 65-80.
- 7 McCulloch, M.T., and Gamble, J., 1991, Geochemical and geodynamical
8 constraints on subduction zone magmatism: Earth and Planetary Science
9 Letters, v. 102, p. 358-374.
- 10 Stolz, A., Jochum, K., Spettel, B., and Hofmann, A., 1996, Fluid-and
11 melt-related enrichment in the subarc mantle: evidence from Nb/Ta
12 variations in island-arc basalts: Geology, v. 24, p. 587-590.
- 13 Sun, S.-S., and McDonough, W.F., 1989, Chemical and isotopic systematics of
14 oceanic basalts: implications for mantle composition and processes:
15 Geological Society, London, Special Publications 42, p. 313-345.
- 16 Tong, X.R., Liu, Y., Hu, Z., Chen, H., Zhou, L., Hu, Q., Xu, R., Deng, L., Chen,
17 C., and Gao, S., 2015, Accurate Determination of Sr Isotopic
18 Compositions in Clinopyroxene and Silicate Glasses by
19 LA-MC-ICP-MS: Geostandards and Geoanalytical Research, v. 40, p.
20 85-89.
- 21 Vermeesch, P., 2006, Tectonic discrimination diagrams revisited:
22 Geochemistry Geophysics Geosystems, v. 7, p. Q06017.

- 1 Wang, Q.H., Yang, H., Yang, D.B., and Xu, W.L., 2014, Mid-Mesoproterozoic
2 (~ 1.32 Ga) diabase swarms from the western Liaoning region in the
3 northern margin of the North China Craton: Baddeleyite Pb–Pb
4 geochronology, geochemistry and implications for the final breakup of the
5 Columbia supercontinent: *Precambrian Research*, v. 254, p. 114-128.
- 6 Wang, Y., Qiu, Y., Gao, J., and Zhang, Q., 2003, Proterozoic anorogenic
7 magmatic rocks and their constraints on mineralizations in the Bayan Obo
8 deposit region, Inner Mongolia: *Science in China (D)*, v. 46, p. 26-40.
- 9 Yang, K.F., Fan, H.R., Santosh, M., Hu, F.F., and Wang, K.Y., 2011,
10 Mesoproterozoic mafic and carbonatitic dykes from the northern margin of
11 the North China Craton: implications for the final breakup of Columbia
12 supercontinent: *Tectonophysics*, v. 498, p. 1-10.
- 13 Yang, Y.H., Sun, J.F., Xie, L.W., Fan, H.R., and Wu, F.Y., 2008, In situ Nd
14 isotopic measurement of natural geological materials by LA-MC-ICPMS:
15 *Chinese Science Bulletin*, v. 53, p. 1062-1070.
- 16 Zhang, H.F., Sun, M., Zhou, X.H., Zhou, M.F., Fan, W.M., and Zhang, J.P.,
17 2003, Secular evolution of the lithosphere beneath the eastern North
18 China Craton: evidence from Mesozoic basalts and high-Mg andesites:
19 *Geochimica et Cosmochimica Acta*, v. 67, p. 4373-4387.
- 20 Zhang, M., Suddaby, P., Thompson, R.N., Thirlwall, M.F., and Menzies, M.A.,
21 1995, Potassic volcanic rocks in NE China: geochemical constraints on
22 mantle source and magma genesis: *Journal of Petrology*, v. 36, p.

1 1275-1303.

2 Zhang, S.H., Zhao, Y., and Santosh, M., 2012, Mid-Mesoproterozoic bimodal
3 magmatic rocks in the northern North China Craton: implications for
4 magmatism related to breakup of the Columbia supercontinent:
5 Precambrian Research, v. 222-223, p. 339-367.

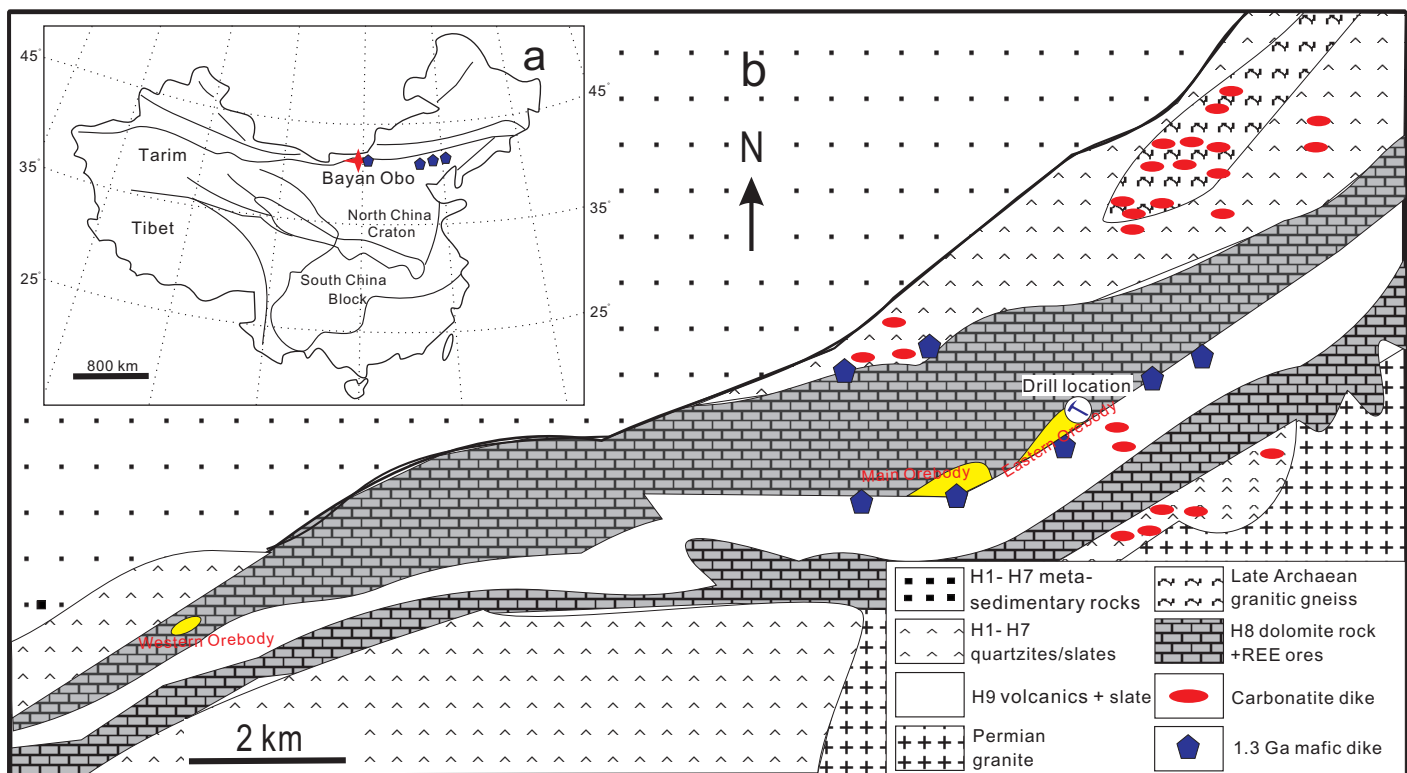


Figure DR1

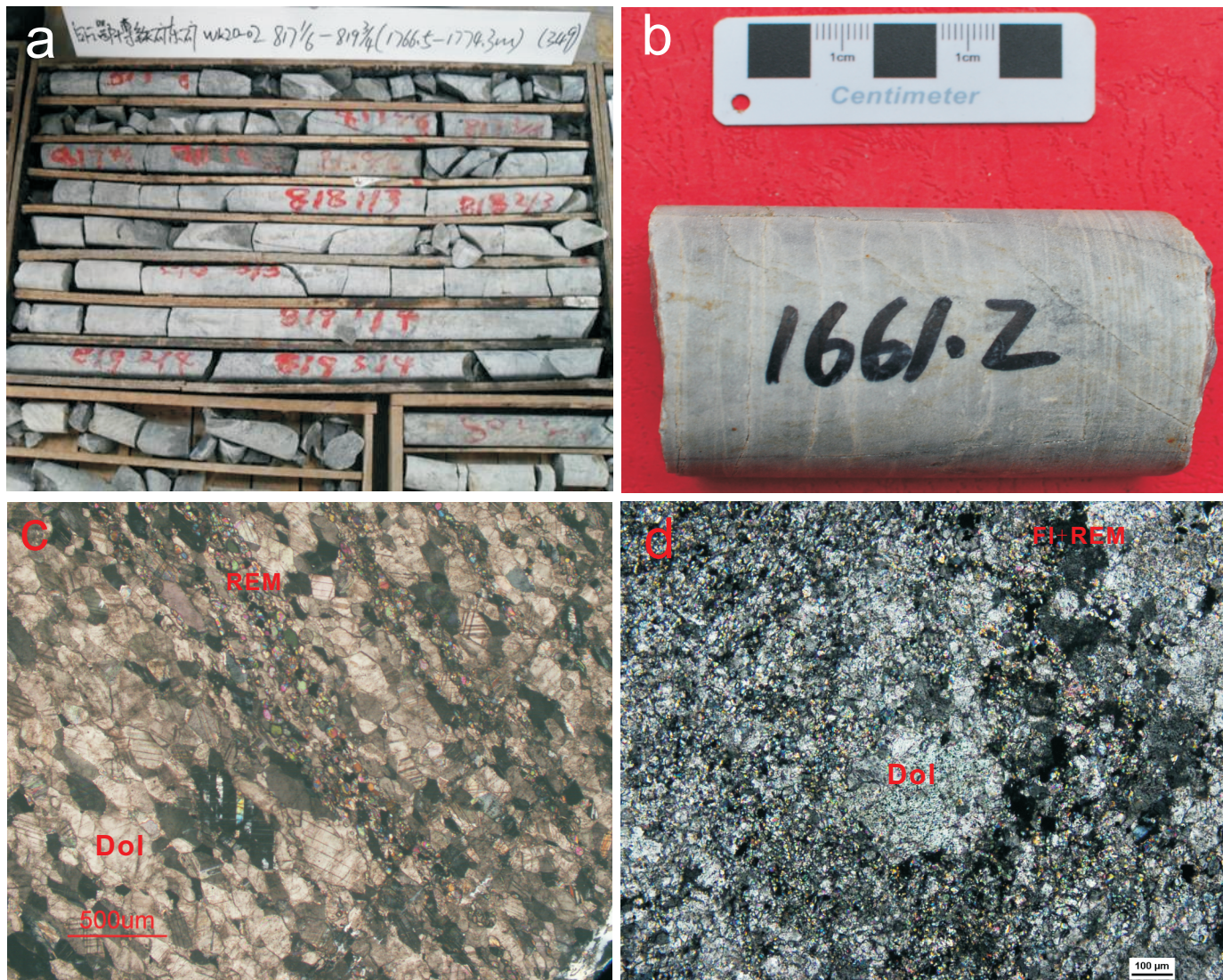


Figure DR2

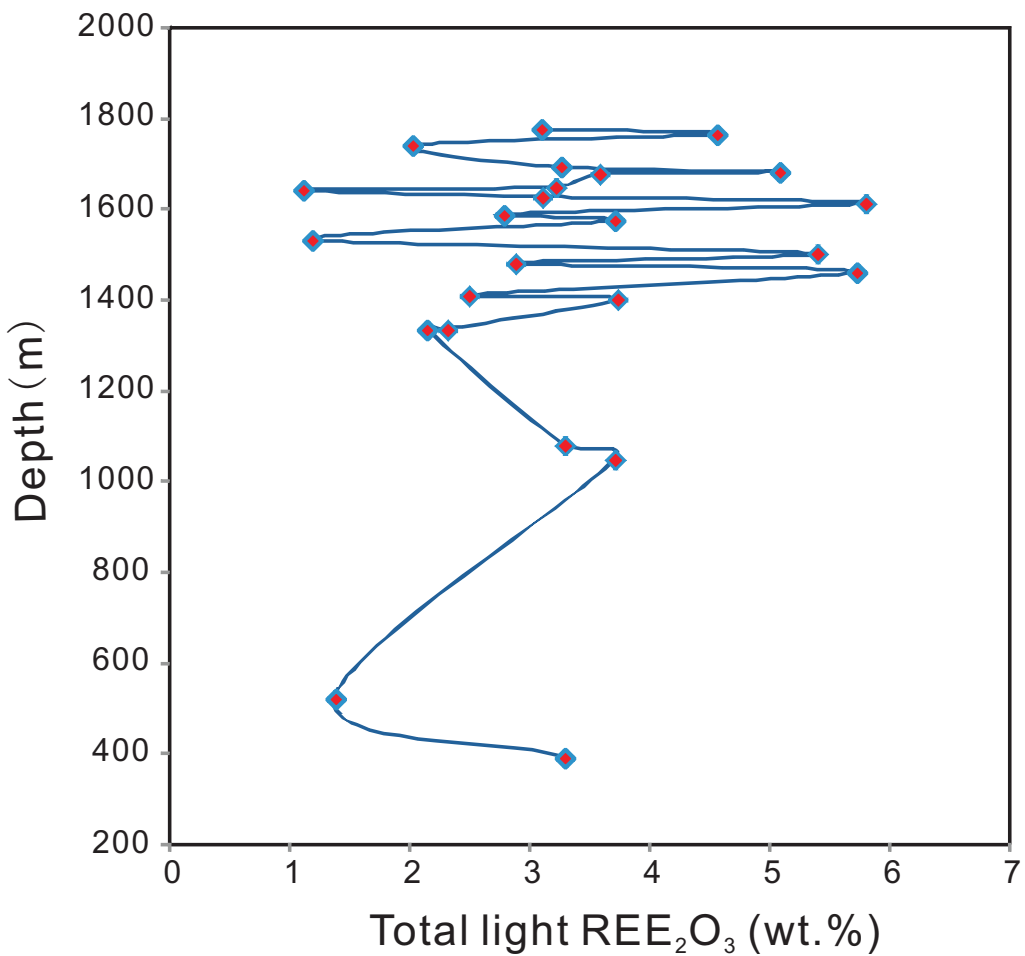


Figure DR3

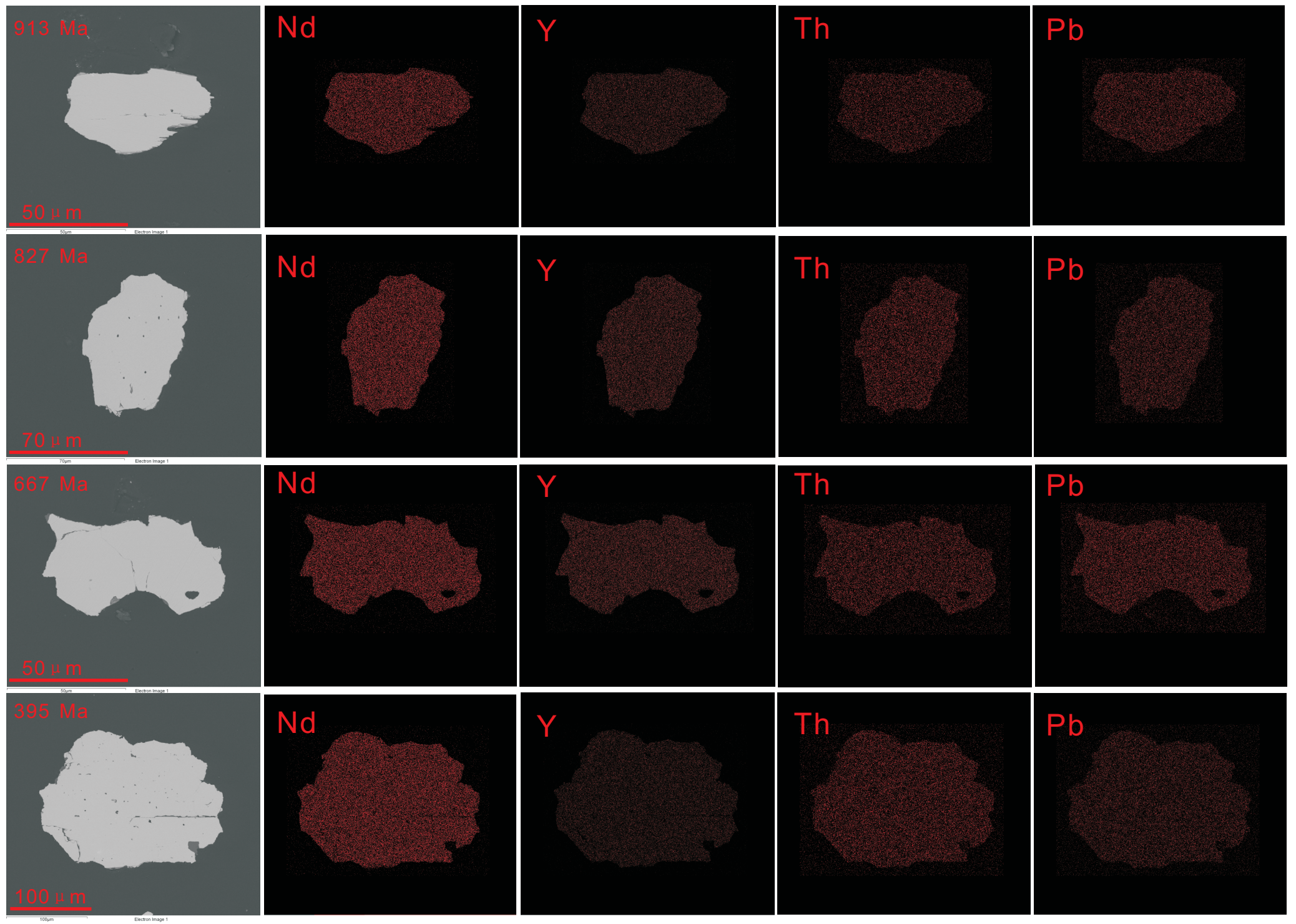


Figure DR4

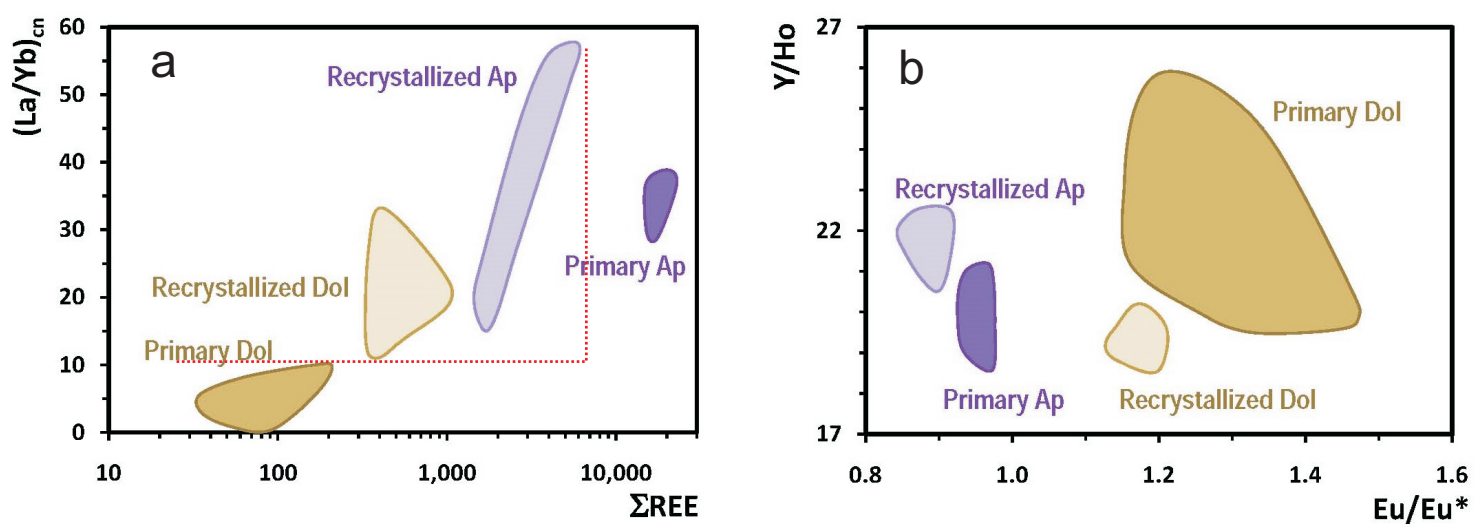


Figure DR5

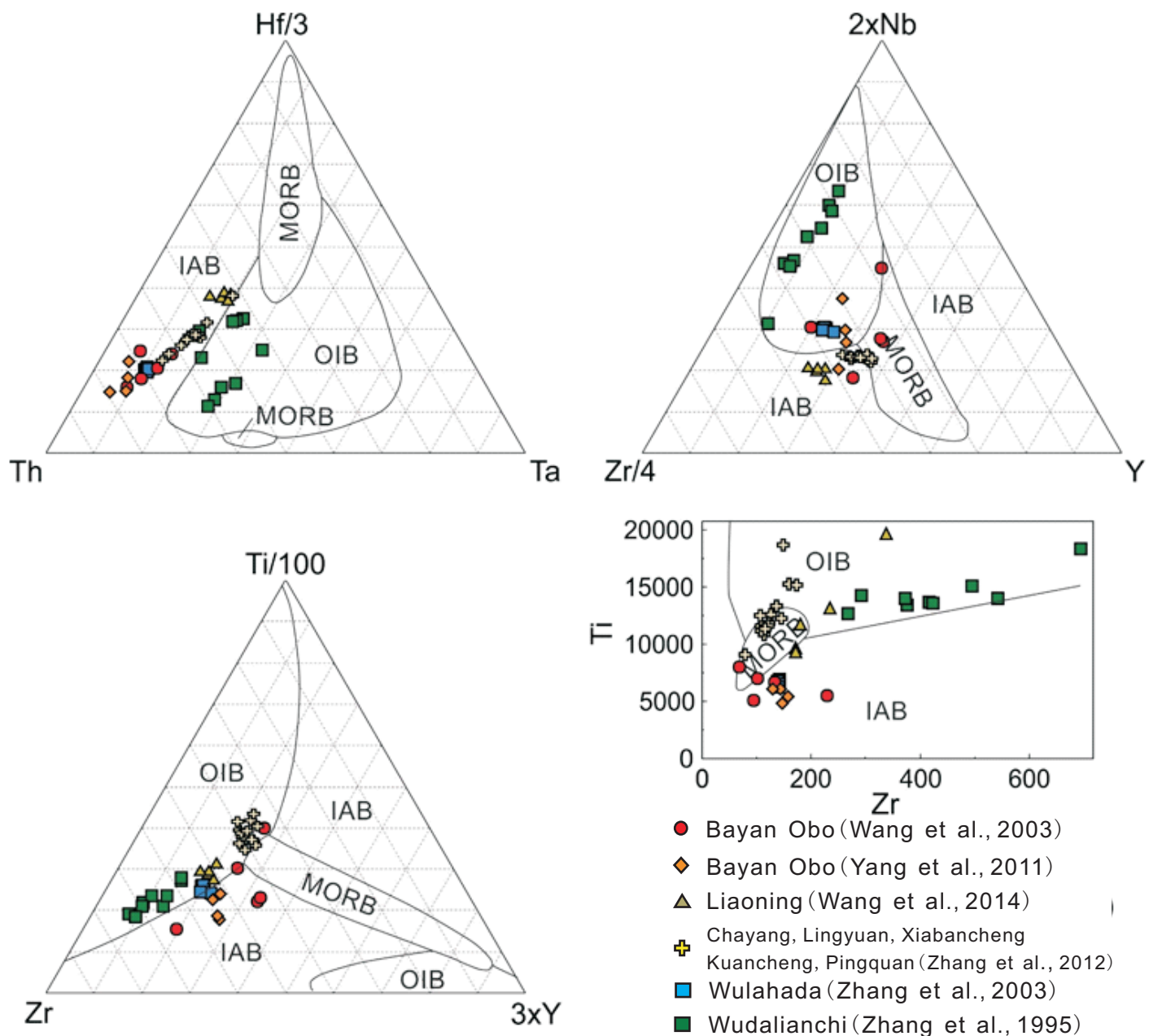


Figure DR6

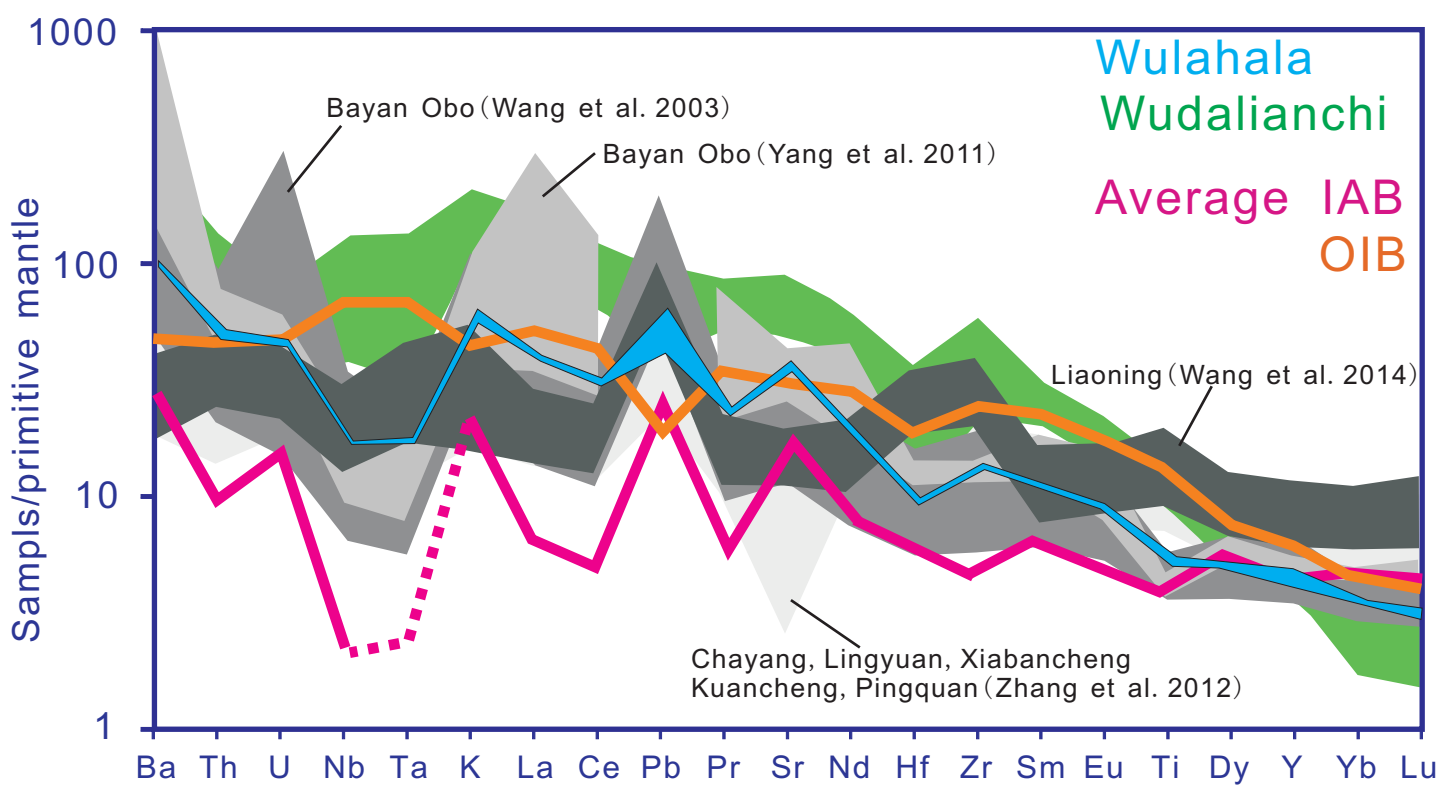


Figure DR7

Table DR1. Chemical compositions (wt.%) in Bayan Obo drill cores with different depths

Depth(m)	TiO ₂	Al ₂ O ₃	FeO	MgO	CaO	MnO	Na ₂ O	K ₂ O	P ₂ O ₅	BaO	SrO	La ₂ O ₃	Ce ₂ O ₃	Pr ₂ O ₃	Nd ₂ O ₃	Sm ₂ O ₃
392	0.03	0.06	17.20	13.53	30.91	4.30	0.08	0.04	0.04	0.07	0.26	0.67	1.67	0.21	0.68	0.06
520	0.06	0.03	6.55	18.65	32.03	1.77	0.07	0.02	0.23	0.44	0.52	0.36	0.69	0.08	0.24	0.02
1048	0.08	0.98	12.23	13.44	24.58	2.35	1.81	1.72	0.31	0.05	0.63	0.93	2.07	0.20	0.47	0.03
1080	0.05	1.59	7.69	13.89	27.33	2.72	0.04	1.89	1.85	0.20	0.23	0.59	1.55	0.22	0.84	0.09
1336	0.04	0.14	7.74	14.62	31.25	2.60	0.08	0.06	1.97	0.99	0.31	0.57	1.05	0.12	0.37	0.03
1336	0.04	0.06	7.74	14.62	31.25	1.76	0.08	0.01	2.54	0.15	0.46	0.56	1.10	0.13	0.46	0.05
1402	0.02	0.07	5.36	14.37	32.16	1.84	0.03	0.03	3.07	0.06	0.19	1.26	1.81	0.17	0.45	0.04
1410	0.02	0.07	8.48	17.69	34.62	2.29	0.03	0.02	1.36	0.04	0.17	0.67	1.25	0.13	0.40	0.04
1461	0.06	0.06	8.38	17.22	33.60	1.74	0.07	0.02	0.63	0.03	0.81	1.79	2.85	0.28	0.74	0.06
1480	0.05	0.10	7.47	12.17	29.23	1.51	0.05	0.02	5.86	0.13	0.49	0.75	1.41	0.16	0.50	0.06
1502	0.06	0.09	7.95	12.92	29.40	1.47	0.03	0.01	2.35	0.15	0.47	1.62	2.61	0.27	0.81	0.08
1532	0.03	0.05	7.65	13.67	27.45	1.47	0.03	0.01	0.36	0.59	0.26	0.33	0.58	0.06	0.19	0.02
1574	0.05	0.04	8.36	16.55	29.48	1.93	0.02	0.01	0.12	1.30	0.35	1.12	1.82	0.19	0.53	0.05
1588	0.36	0.35	13.48	15.07	27.19	2.33	0.06	0.32	1.90	1.86	0.49	0.65	1.41	0.17	0.51	0.05
1612	0.06	0.09	6.52	16.30	38.86	1.32	0.04	0.05	3.34	0.49	0.39	2.00	2.78	0.27	0.69	0.06
1627	0.25	0.26	13.53	14.76	26.04	2.15	0.03	0.29	1.43	0.22	0.30	0.93	1.56	0.16	0.42	0.04
1641	0.02	0.08	11.30	15.65	28.88	2.38	0.05	0.01	0.63	0.18	0.16	0.29	0.55	0.06	0.19	0.02
1649	0.05	0.71	6.69	11.81	36.17	2.08	0.08	0.34	2.14	0.24	0.23	1.08	1.57	0.15	0.38	0.04
1676	0.02	0.07	8.67	14.67	30.31	1.66	0.28	0.10	0.19	0.39	0.57	1.14	1.81	0.17	0.42	0.03
1683	0.06	0.29	6.81	15.30	25.16	1.73	0.30	0.46	2.09	0.53	0.81	1.67	2.46	0.24	0.65	0.05
1692	0.06	0.21	7.40	17.60	27.45	1.48	0.10	0.40	0.75	0.99	0.83	0.91	1.70	0.17	0.44	0.04
1740	0.04	0.12	10.55	15.58	28.96	1.54	0.25	0.25	0.05	1.10	0.50	0.52	0.99	0.11	0.36	0.03
1765	0.13	0.08	9.40	12.52	35.01	1.47	0.08	0.06	2.43	0.06	0.25	1.12	2.41	0.26	0.71	0.06
1776	0.03	0.03	6.71	14.40	34.55	1.30	0.11	0.02	1.64	0.62	0.24	0.91	1.52	0.16	0.46	0.04

Table DR2. Monazite dating data from the drill cores in Bayan Obo

sample	Th(ppm)	U(ppm)	Th/U	$^{208}\text{Pb}/^{232}\text{Th}$	σ	Pb/Th age(Ma)	σ
BO-1	2308	3.57	646	0.0462	1.7	913	15
BO-2	4197	1.03	4080	0.0438	1.7	866	14
BO-3	2506	3.04	825	0.0415	1.9	822	16
BO-4	1841	2.19	839	0.0410	1.6	811	13
BO-5	2138	2.93	729	0.0401	1.6	795	13
BO-6	2056	2.60	792	0.0400	1.7	792	13
BO-7	1987	2.32	858	0.0377	1.6	748	12
BO-8	2889	2.08	1389	0.0333	1.8	662	12
BO-9	1783	2.19	815	0.0318	1.9	633	12
BO-10	1436	0.97	1488	0.0288	1.9	573	11
BO-11	2294	2.56	897	0.0285	1.6	569	9
BO-12	1551	1.71	907	0.0280	2.5	558	14
BO-13	1302	2.55	511	0.0266	1.6	530	9
BO-14	3134	1.58	1979	0.0259	1.6	517	8
BO-15	4817	1.32	3643	0.0224	2.2	448	10
BO-16	2654	<0.1	>10000	0.0206	1.6	413	7
BO-17	2407	<0.1	>10000	0.0206	1.7	413	7
BO-18	2230	<0.1	>10000	0.0206	2.0	411	8
BO-19	2934	<0.1	>10000	0.0205	1.8	410	7
BO-20	2307	<0.1	>10000	0.0204	1.8	408	8
BO-21	1709	1.68	1015	0.0203	1.6	406	7
BO-22	3272	1.42	2312	0.0197	1.8	394	7
BO-23	1482	1.83	812	0.0185	1.7	370	6
BO-24	1530	1.30	1177	0.0180	1.6	361	6

Table DR3. In-situ Nd isotope of monazites from Bayan Obo drill cores

sample	$^{147}\text{Sm}/^{144}\text{Nd}$	2σ	$^{143}\text{Nd}/^{144}\text{Nd}$	2σ	age (Ma)	$\varepsilon_{\text{Nd}}(t)^{\#}$	$T_{\text{CHUR}}(\text{Ga})$
BO-1	0.04239	2	0.511362	19	913	-6.9	1.59
BO-2	0.04607	5	0.511358	32	866	-8.3	1.63
BO-3	0.04606	2	0.511319	22	822	-9.9	1.66
BO-4	0.04487	4	0.511348	23	811	-9.4	1.62
BO-5	0.04645	4	0.511316	27	795	-10.5	1.67
BO-6	0.04651	5	0.511348	22	792	-10.0	1.64
BO-7rim	0.04363	8	0.511309	37	748	-11.3	1.65
BO-7rim	0.04320	4	0.511305	39	748	-11.3	1.65
BO-7core	0.04349	6	0.511318	41	748	-11.1	1.64
BO-7core	0.04633	4	0.511377	25	748	-10.2	1.61
BO-8	0.04561	7	0.511372	22	662	-11.9	1.61
BO-9	0.04394	2	0.511346	20	633	-12.9	1.62
BO-10	0.04507	14	0.511353	25	573	-14.0	1.62
BO-11	0.04652	3	0.511346	21	569	-14.3	1.64
BO-12	0.04497	4	0.511339	19	558	-14.5	1.63
BO-13	0.04375	3	0.511345	24	530	-14.9	1.62
BO-14	0.04410	10	0.511341	34	517	-15.2	1.62
BO-15rim	0.03962	8	0.511283	38	448	-17.5	1.63
BO-15core	0.04118	6	0.511326	14	448	-16.7	1.61
BO-16	0.03988	3	0.511342	26	413	-17.0	1.58
BO-17	0.03938	2	0.511365	25	413	-16.5	1.56
BO-18	0.03588	9	0.511334	27	411	-17.0	1.55
BO-19	0.04002	11	0.511355	27	410	-16.8	1.57
BO-20	0.03950	4	0.511360	23	408	-16.8	1.56
BO-21	0.04533	3	0.511362	33	406	-17.1	1.62
BO-22	0.04763	20	0.511361	24	394	-17.4	1.64
BO-23	0.04527	3	0.511351	27	370	-18.0	1.62
BO-24core	0.04619	7	0.511377	22	361	-17.7	1.61
BO-24rim	0.04616	2	0.511376	23	361	-17.7	1.61

[#] $\varepsilon_{\text{Nd}}(t)$ values are calculated based on present-day $(^{147}\text{Sm}/^{144}\text{Nd})_{\text{CHUR}} = 0.1967$ and $(^{143}\text{Nd}/^{144}\text{Nd})_{\text{CHUR}} = 0.512638$.

Table DR4. In-situ trace element compositions (ppm) of dolomite and apatite from Bayan Obo drill cores

dolomite	primary												recrystallization				
Rb	0.05	bdl [#]	bdl	bdl	bdl	bdl	bdl	0.09	bdl	bdl	0.01	0.01	0.02	0.01	0.03	0.04	
Sr	1766	1528	1818	2228	2174	2559	2671	2429	1197	2640	2738	4294	4513	4378	4559	4451	4289
Ba	67.5	9.34	86.1	13.4	133	124	561	90.1	106	69.4	39.5	43.5	61.6	58.3	33.6	56.0	55.5
Y	23.3	28.8	25	27.9	17.3	13.0	19.3	9.31	23.1	31.5	29.6	56.2	58.3	65.3	105.8	78.4	62.0
La	7.18	3.59	9.17	4.92	5.25	5.06	9.63	3.61	15.5	65.7	27.4	36.6	36.6	56.5	109	101	73.8
Ce	25.2	14.0	25.9	17.3	11.2	10.4	19.6	7.69	54.8	162	62.0	128	136	192	362	314	234
Pr	3.83	2.16	3.65	2.58	1.39	1.16	2.36	0.93	7.50	15.1	7.50	17.8	19.6	26.3	51.8	43.1	31.4
Nd	16.9	11.3	16.6	13.4	5.93	5.9	11.4	4.46	32.4	65.3	33.6	77.4	85.2	112	222	184	136
Sm	5.03	3.37	4.10	3.94	1.52	2.67	4.69	1.81	6.54	17.1	8.94	17.9	20.4	24.8	47.3	37.0	28.4
Eu	2.03	1.60	1.99	1.71	0.73	1.15	1.79	0.84	2.47	6.35	3.36	6.52	7.67	8.64	16.3	12.5	9.60
Gd	3.99	3.48	4.12	3.73	1.75	2.46	4.45	2.44	4.79	14.5	7.22	15.3	17.5	19.6	36.8	28.1	21.7
Tb	0.90	0.81	0.76	0.69	0.42	0.41	0.95	0.40	0.85	2.24	1.30	2.84	3.38	3.68	6.45	5.0	3.92
Dy	5.61	6.23	5.31	5.16	2.82	2.86	4.75	2.26	5.17	10.3	6.85	16.2	18.1	20.1	33.7	26.1	20.1
Ho	1.16	1.32	1.23	1.24	0.79	0.53	0.92	0.36	0.90	1.69	1.28	2.8	3.0	3.38	5.5	4.11	3.23
Er	2.89	4.08	3.17	3.37	1.95	1.30	1.89	0.78	2.37	3.07	3.35	5.41	5.72	6.43	10.1	7.40	5.52
Tm	0.35	0.61	0.43	0.38	0.40	0.17	0.23	0.10	0.25	0.32	0.39	0.55	0.53	0.58	0.87	0.64	0.55
Yb	2.01	3.31	2.74	2.03	2.31	0.79	1.17	0.53	1.38	1.39	2.0	2.18	2.18	2.50	3.75	2.90	2.24
Lu	0.20	0.39	0.22	0.17	0.29	0.11	0.14	0.04	0.17	0.12	0.22	0.18	0.20	0.23	0.32	0.21	0.21

Table DR4. continued

apatite		primary								recrystallization			
Rb	0.14	1.40	0.26	0.26	3.01	0.10	0.08	0.04	0.12	0.14	0.12	0.48	0.18
Sr	5109	4026	5006	4586	3982	2834	2663	2956	2942	2364	3257	3255	3223
Ba	22.9	22.7	62.4	35.3	17	83	94	133	204	78.2	64.3	66.7	223
Y	1356	1153	1246	1193	1107	128	102	121	116	144	183	212	119

La	2133	1598	1918	1553	1412	158	157	202	241	564	495	846	339
Ce	7601	5809	6852	5646	6075	585	525	684	779	1505	1387	2372	1114
Pr	1188	937	1035	912	1004	96.7	82	104	109	228	187	335	146
Nd	5830	4406	4954	4553	5151	500	405	516	517	982	827	1394	647
Sm	1227	902	1051	947	1059	106	88.4	103	100	161	144	208	116
Eu	338	251	287	265	278	26.0	21.3	25.5	24.8	37.2	35.9	49.2	27.1
Gd	800	620	714	675	680	61.6	52.8	61.7	60.6	89.5	85.2	116	67.8
Tb	102	76.6	90.0	83.5	78.7	6.75	5.6	6.55	6.05	8.35	9.24	11.5	7.06
Dy	497	376	451	417	377	36.3	29.3	34.2	31.9	40.9	49.4	58.2	33.5
Ho	72.3	54.7	65.9	61.6	53.6	5.79	4.68	5.85	5.38	6.51	8.17	9.48	5.47
Er	132	102	124	118	99.9	13.8	10.7	12.8	12.4	14.7	19.0	22.5	12.1
Tm	11.1	8.50	10.3	9.92	8.02	1.45	1.07	1.37	1.42	1.53	1.94	2.19	1.21
Yb	38.9	30.3	37.1	36.8	28.9	6.76	5.25	6.1	6.95	7.24	8.45	10.3	5.89
Lu	3.07	2.40	2.98	3.03	2.35	0.63	0.50	0.61	0.79	0.70	0.78	0.99	0.58

#below determination limits.

Table DR5. In-situ Sr isotope of dolomite and apatite from Bayan Obo drill cores

dolomite				apatite			
primary	recrystallization		primary	recrystallization			
$^{87}\text{Sr}/^{86}\text{Sr}$	2 σ	$^{87}\text{Sr}/^{86}\text{Sr}$	2 σ	$^{87}\text{Sr}/^{86}\text{Sr}$	2 σ	$^{87}\text{Sr}/^{86}\text{Sr}$	2 σ
0.70250	25	0.70606	33	0.70296	19	0.70351	8
0.70241	20	0.70669	67	0.70294	17	0.70323	19
0.70238	22	0.70384	22	0.70293	23	0.70345	13
0.70271	12	0.70946	53	0.70297	19	0.70349	7
0.70293	16	0.70760	81	0.70297	34	0.70357	16
0.70287	9	0.70456	35			0.70357	18
0.70290	14	0.70786	50			0.70367	11
0.70280	9	0.70682	21			0.70347	14
0.70297	10	0.70572	10			0.70347	12
0.70284	14	0.70971	19			0.70364	18
0.70290	9	0.70889	10			0.70341	13
0.70289	4	0.70871	17			0.70354	13
0.70281	9	0.70533	14				
0.70282	5	0.70568	23				
0.70295	8	0.70827	26				
0.70294	3	0.70718	35				
0.70285	7	0.70467	11				
0.70279	4						